Journal of Drive and Control, Vol.18 No.4 pp.84-90 Dec. 2021
ISSN 2671-7972(print) ISSN 2671-7980(online)
http://dx.doi.org/10.7839/ksfc.2021.18.4.084

Optimum Hydraulic Oil Viscosity Based on Slipper Model Simulation for Swashplate Axial Piston Pumps/Motors

Toshiharu Kazama[1*]

Received: 25 Nov. 2021, Accepted: 26 Nov. 2021

Key Words: Tribology, Hydraulic oil, Viscosity, Thermohydrodynamic lubrication, Slipper, Piston machine, Optimal design

Abstract: Viscosity of hydraulic oils decreases due to loss reduction and efficiency increase of fluid power systems. However, low viscosity is not always appropriate due to the induction of large leakage and small lubricity. Therefore, a detailed study on the optimum viscosity of hydraulic oils is necessary. In this study, based on the thermohydrodynamic lubrication theory, numerical simulation was conducted using the slipper model of swashplate-type axial piston pumps and motors. The viscosity grades' (VG) effects of oils on power losses are mainly discussed numerically in fluid film lubrication, including changes in temperature and viscosity. The simulation results reveal that the flow rate increases and the friction torque decreases as VG decreases. The film temperature and power loss were minimised for a specific oil with a VG. The minimum conditions regarding the temperature and loss were different and closed. Under various operating conditions, the film temperature and power loss were minimised, suggesting that an optimum hydraulic oil with a specific VG could be selected for given operating conditions of pressure and speed. Otherwise, a preferable operating condition must be established to determine a specific VG oil.

Nomenclature

a: recess radius ratio, $= R_1/R_2$
B: pad thickness, m
B_i: parameter, $= Bh_T/\lambda'$
c_p: specific heat at constant pressure, J/(kg·K)
E_c: parameter, $= (\omega R_2)^2/(c_p T_0)$
H: representative clearance, m
$\bar{h}$: clearance, $= h/H$
$\bar{h}_c$: centre clearance, $= h_c/H$
h_T: heat transfer coefficient, W/(m·K)
$\bar{L}$: power loss, $= L/(\omega p_s {R_2}^3 So)$
$\bar{M}$: moment, $= M/(p_s {R_2}^3 So)$
Nu: parameter, $= Hh_T/\lambda$
Pe': parameter, $= PrRe'$
Pr: parameter, $= \mu_0 c_p/\lambda$
p: pressure, $= p/(p_s So)$
p_r: recess pressure, $= p_r/(p_s So)$
p_s: supply pressure, Pa
$\bar{Q}$: flow rate, $= Q/(\omega {R_2}^3)$
Q_{out}: leakage flow rate, m^3/s
Re': parameter, $= \rho\omega H^2/\mu_0$
$\bar{R}_0$: revolution radius, $= R_0/R_2$
R_1: recess radius, m
R_2: pad outer radius, m
r, θ, z: cylindrical coordinates, $= r/R_2, \theta, z/H$
r_w: load eccentricity, m
So: parameter, $= 6\mu_0\omega(R_2/H)^2/p_s$
$\bar{T}$: temperature, $= T/T_0$
$\bar{T}_a$: ambient temperature, $= T_a/T_0$
$\bar{T}_f$: friction torque, $= T_f/(p_s {R_2}^3 So)$
$\bar{T}_r$: recess temperature, $= T_r/T_0$
$\bar{T}_s$: supply oil temperature, $= T_s/T_0$
T_0: reference temperature, K
$\bar{u}, v, \bar{w}$: velocities, $= u/(\omega R_2), v/(\omega R_2), w/(\omega H)$
$\bar{W}$: load, $= W/(p_s {R_2}^2 So)$
X, Y, Z: orthogonal coordinates on disk
x, y, z: orthogonal coordinates on slipper
$\bar{\alpha}$: pad inclination angle, $= \alpha R_2/H$
λ: thermal conductivity of oil, W/(m·K)
λ': thermal conductivity of pad, W/(m·K)

* Corresponding author: kazama@mmm.muroran-it.ac.jp
1 College of Design and Manufacturing Technology, Graduate School of Muroran Institute of Technology, Hokkaido, 050-8585, Japan
Copyright Ⓒ 2021, KSFC
This is an Open-Access article distributed under the terms of the Creative Commons Attribution Non-Commercial License(http://creativecommons.org/licenses/by-nc/3.0) which permits unrestricted non-commercial use, distribution, and reproduction in any medium, provided the original work is properly cited.

μ: viscosity, $= \mu/\mu_0$
ν: kinematic viscosity, m^2/s
ρ: density, kg/m^3
$\bar{\Phi}$: angle, $= \Phi R_2/H$
ϕ: maximum pad azimuth, rad
Ω: reference angular velocity, rad/s
Ω': sliding angular velocity, rad/s
ω: pad angular velocity, rad/s

Subscripts
0: reference (high pressure period)

1. Introduction

Hydraulic systems are widely used in the construction, aviation and manufacturing industries because they can effectively transfer energy or power with high efficiency, responsivity and flexibility[1]. A large amount of power can be transmitted using hydraulic equipment with high pressure, linking the low efficiency of pumps and actuators to large losses[2].

Selection of hydraulic oil with appropriate viscosity is a way of improving efficiency because viscosity dictates the physical properties of oils[3], particularly in terms of lubrication and leakage that are directly related to mechanical and volumetric losses[4]. Generally, high viscosity causes mechanical loss, whereas, low viscosity causes volumetric loss. Since the total loss is the summation of mechanical and volumetric losses, an optimal viscosity may exist, e.g., the kinematic viscosity (ν) equivalent at 40°C is about 43–172 mm^2/s empirically for axial piston pumps[5], although the preferable and optimum viscosity of hydraulic oils depends on pumps, motors, systems and operation.

Recently, the viscosity of hydraulic oils decreases owing to flow loss in pipes[4] and churning loss in components. However, a low viscosity may not always be appropriate owing to the induction of less sealing effect and small hydrodynamic pressure, resulting in large leakage and solid contact and subsequently low volumetric efficiency and wear and seizure. Therefore, a detailed study of the optimum viscosity of hydraulic oils is necessary.

An appropriate oil with an optimum viscosity grade (VG) for a hydraulic system does not exist because a circuit of systems consists of several components including hydraulic pumps, valves, pipes, actuators and auxiliary components, having different flow behaviours and functions. Among them, hydraulic pumps and motors are the main components; thus, the losses in such components largely degrade their performances and the efficiency of a system[6].

Hydraulic pumps and motors are positive displacement machines, whose performance depends on the tribological characteristics of sliding parts. For piston pumps and motors, prime parts are the interfaces between the pistons and cylinder bores[7-8], the cylinder block and valve plate[9-10] and the slippers and swashplate[11-12]. Precisely, the oil viscosity and the lubrication characteristics affect interface between slippers and a swashplate because of the severe operating conditions of high load and speed. Sliding parts are heated by viscous dissipation in a thin fluid film, increasing oil temperature. Because viscosity varies with temperature, viscosity distribution becomes uneven owing to temperature variation. Since viscosity is determined by a reference ν at a specific temperature, e.g. 40°C (oil VG) and oil temperature (viscosity–temperature relation), accurate estimation of temperature distributions and appropriate selection of the oil VG are important.

The theoretical approach regarding thermal lubrication behaviour is the thermohydrodynamic lubrication (THL) theory[13]. Several theoretical and experimental studies of THL have been conducted mainly for hydrodynamic bearings rather than hydrostatic bearings[14]. Therefore, a model of hybrid (hydrostatic and hydrodynamic) thrust bearings, including the changes in physical properties of oils, was developed[15]. This model applies to a slipper installed in swashplate-type axial piston pumps and motors, suitable for thermal lubrication analysis of hydraulic equipment.

In this study, we investigate the thermal lubrication characteristics of a slipper relating to the oil VG and conduct a numerical simulation using the THL model between a slipper and a swashplate of axial piston pumps and motors[16]. Based on the optimum design of the components[17], oil VG effects on the slipper characteristics including flow leakage, friction torque, film temperature and power losses in fluid film lubrication are discussed.

2. Theory

2.1 Theoretical model

The schematic of the THL slipper model is shown in Fig. 1[14]. The basic equations consisting mainly of the Reynolds, energy and heat conduction equations are given by

$$\frac{1}{r}\frac{\partial}{\partial r}\left(\bar{F}_2\bar{h}^3 r\frac{\partial p}{\partial r}\right)+\frac{1}{r^2}\frac{\partial}{\partial \theta}\left(\bar{F}_2\bar{h}^3\frac{\partial p}{\partial \theta}\right)$$

$$=\omega\frac{\partial}{\partial\theta}\left(\frac{\bar{F}_3\bar{h}}{\bar{F}_0}\right)+\bar{\Omega}\bar{R}_0\sin\theta\frac{\partial\left(\bar{F}_4\bar{h}\right)}{\partial r}$$

$$+\bar{\Omega}\left(\frac{\bar{R}_0}{r}\sin\theta+1\right)\frac{\partial\left(\bar{F}_4\bar{h}\right)}{\partial\theta} \quad (1)$$

with

$$\begin{cases} \bar{F}_0 = \int_0^1 \dfrac{dz}{\mu} \\ \bar{F}_1 = \int_0^1 \dfrac{z dz}{\mu} \\ \bar{F}_2 = -6\left(\int_0^1 \int_0^z \dfrac{dz}{\mu} dz - \bar{F}_1 \dfrac{\bar{F}_3}{\bar{F}_0}\right) \\ \bar{F}_3 = \int_0^1 \int_0^z \dfrac{dz}{\mu} dz \end{cases} \quad (2),$$

$$\left[u\left(\frac{\partial \bar{T}}{\partial r} - m_r \frac{\partial \bar{T}}{\partial z}\right) + \frac{v}{r}\left(\frac{\partial \bar{T}}{\partial \theta} - m_\theta \frac{\partial \bar{T}}{\partial z}\right) + \frac{w}{\bar{h}}\frac{\partial \bar{T}}{\partial z}\right] = \frac{1}{Pe'}\frac{\partial}{\bar{h}^2 \partial z}\left(\bar{\lambda}\frac{\partial \bar{T}}{\partial z}\right) + \frac{Ec}{Re'}\mu\varphi \quad (3)$$

with

$$\begin{cases} m_r = \dfrac{z}{\bar{h}}\dfrac{\partial \bar{h}}{\partial r} \\ m_\theta = \dfrac{z}{\bar{h}}\dfrac{\partial \bar{h}}{\partial \theta} \end{cases} \quad (4)$$

and

$$\phi = \frac{1}{\bar{h}^2}\left[\left(\frac{\partial \bar{u}}{\partial z}\right)^2 + \left(\frac{\partial v}{\partial z}\right)^2\right] \quad (5)$$

and

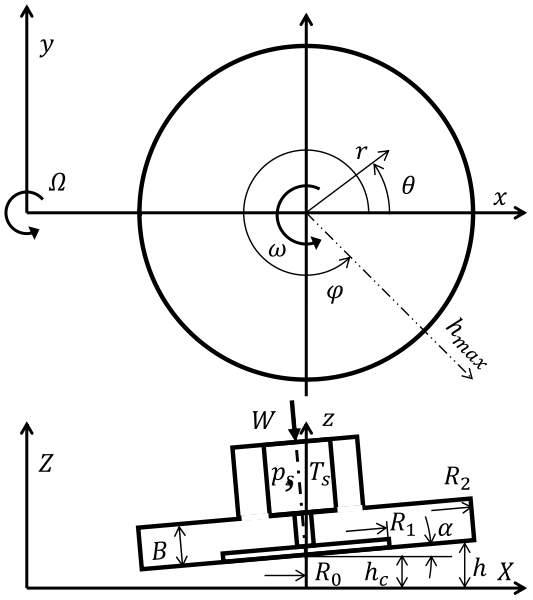

Fig. 1 Schematic of the slipper model

$$\frac{1}{r'}\frac{\partial}{\partial r'}\left(r' \frac{\partial \bar{T}'}{\partial r'}\right) + \frac{1}{r'^2}\frac{\partial^2 \bar{T}'}{\partial \theta^2} + \left(\frac{R_2}{B}\right)^2 \frac{\partial^2 \bar{T}'}{\partial z'^2} = 0 \quad (6).$$

In the following simulation, viscosity is treated as a function of temperature only although density, specific heat, thermal conductivity and viscosity are functions of temperature and pressure. Additionally, the thermal expansivity of oils is neglected in the energy equation.

The kinematic viscosity (ν) is estimated using the following Walther equation.

$$\log\log(\nu^\dagger + c) = -m \log T^\dagger + b \quad (7)$$

where $\nu^\dagger$ is the kinematic viscosity in mm^2/s, $T^\dagger$ is the absolute temperature in K, b and m are specific constants depending on each oil and c is set at 0.7.

The boundary conditions of Eq. (1) for pressure and Eqs. (3) and (6) for temperature are given by

$$\begin{cases} p(a,\theta) = p_r \\ p(1,\theta) = p_a \end{cases} \quad (8)$$

and

$$\begin{cases} \bar{T}(r,\theta,0) = \bar{T}_w \\ \bar{T}(a,\theta,z) = \bar{T}_r \\ \bar{T}'(a,\theta,z') = \bar{T}_r \\ -\dfrac{\partial \bar{T}'(1,\theta,z')}{\partial r} = \dfrac{R_2}{B} Bi\left[\bar{T}'(1,\theta,z') - \bar{T}_a\right] \\ -\dfrac{\partial \bar{T}'(r,\theta,1)}{\partial z'} = Bi\left[\bar{T}'(r,\theta,1) - \bar{T}_a\right] \\ -\dfrac{\partial \bar{T}'(r,\theta,0)}{\partial z'} = \dfrac{Bi}{Nu}\dfrac{1}{\bar{h}}\dfrac{\partial \bar{T}(r,\theta,1)}{\partial z} \end{cases} \quad (9)$$

In Eq. (3) and the conditions of (9), Bi, Ec, Nu, Pe' and Re' are the Biot, Eckert, Nusselt, Péclet and Reynolds numbers, respectively, and $Pe' = PrRe'$, where Pr represents the Prandtl number.

The clearance between the slipper pad and the disk is

$$\bar{h} = \bar{h}_c + \alpha r \cos(\theta - \phi) \quad (10)$$

The moment load-carrying capacities around the x and y axes ($\bar{M}_{fx}$ and $\bar{M}_{fy}$) and the load-carrying capacity ($\bar{W}_f$) are calculated using

$$\begin{cases} \bar{M}_{fx} = \int_0^{2\pi}\int_a^1 pr^2 \sin\theta \, dr \, d\theta \\ \bar{M}_{fy} = -\int_0^{2\pi}\int_a^1 pr^2 \cos\theta \, dr \, d\theta \\ \bar{W}_f = \int_0^{2\pi}\int_a^1 prdr \, d\theta + \pi a^2 p_r \end{cases} \quad (11)$$

The flow rates ($\bar{Q}$) in the slipper land at radius (r) and flow rate ($\bar{Q}_r$) through the capillary restrictor are given as

$$\bar{Q} = \frac{H}{R_2} r \int_0^{2\pi} \bar{h} \int_0^1 u dz d\theta \quad (12)$$

and

$$\bar{Q}_r = \pi \left(\frac{H}{R_2}\right) \frac{1}{\mu_s} \frac{p_s - p_r}{\beta} \quad (13),$$

respectively, where, μ_s is the viscosity at the restrictor and β is the recess parameter ($= 4H^3 l_c/(3r_c^4)$, where l_c and r_c are the length and radius of the restrictor, respectively). The leakage flow rate ($\bar{Q}_{out}$) can be obtained when $r = 1$ in Eq. (12).

The friction torque ($\bar{T}_f$) is computed using

$$\bar{T}_f = \frac{H}{6R_2} \times \int_0^{2\pi}\int_a^1 \frac{\mu}{\bar{h}} \begin{bmatrix} \left.\frac{\partial u}{\partial z}\right|_{z=0} \sin(\theta - \Theta) \\ + \left.\frac{\partial v}{\partial z}\right|_{z=0} \cos(\theta - \Theta) \end{bmatrix} \bar{R}' \, r dr d\theta \quad (14)$$

with

$$\begin{cases} \Theta = \cos^{-1}\left(\dfrac{\bar{R}_0{}^2 + \bar{R}'{}^2 - r^2}{2\bar{R}_0\bar{R}'}\right) \\ \bar{R}' = \sqrt{r^2 + \bar{R}_0{}^2 - 2r\bar{R}_0\cos(\pi - \theta)} \end{cases} \quad (15)$$

The power loss ($\bar{L}$) can be estimated by summing the losses due to leakage ($\bar{L}_Q$) and friction ($\bar{L}_T$); thus,

$$\bar{L} = \bar{L}_Q + \bar{L}_T = p_s \bar{Q}_{out} + \bar{\Omega}\bar{T}_f \quad (16)$$

where $\bar{\Omega}$ is the sliding angular velocity of the disk.

2.2 Calculation conditions

The Reynolds, energy and heat conduction equations were solved numerically along with pressure and temperature boundary conditions and viscosity–temperature relation of the Walther formula. The equations were discretized using the finite difference method and were solved numerically. Additionally, the THL solutions were compared with the isothermal (ISO) solutions.

Table 1 lists the five hydraulic oil models designated as VG 22, 32, 46, 68 and 100 that are relatively used in general and distributed in the market. The table also includes the density (ρ) and ν of the oils. The specific heat at constant pressure and thermal conductivity of all oils were assumed as 2000 J/(kg·K) and 0.13 W/(m·K), respectively, although these properties must be somewhat different because of the VG dependency. Under these fluid models, the coefficients of the Walther equation, *m* and *b*, are specified using Table 1 as m = 3.760, 3.729, 3.654, 3.615 and 3.477 and b = 9.521, 9.487, 9.341, 9.285 and 8.985 for VG 22, 32, 46, 68 and 100, respectively.

Further, the representative geometrical and operating parameters are the pad radius (R_2), recess radius ratio (a) and pad thickness (B) of 10, 0.7 and 5 mm, respectively. The load eccentricity ratio (r_w/R_2), revolution radius ratio (R_0/R_2) and normalised load (hydrostatic balance ratio) (ζ)[18] are 0.1, 3 and 0.9, respectively. The thermal conductivity and heat transfer coefficient of the pad are 50 W/(m·K) and 50 W/(m^2·K), respectively.

3. Results and discussion

3.1 Kinematic viscosity of the lubricant models

Figure 2 shows the temperature dependence of ν with VG 22–100 for the hydraulic oils. Owing to the viscosity–temperature relation, the ν of higher VG oils at high temperature is close to the ν of lower VG at low temperature. Thus, if ν at 40°C of VG 32 (32.6 mm^2/s) is selected as the reference, the same ν for VG 22, 46, 68 and 100 are obtained at 31.6°C, 47.9°C, 56.7°C and 66.8°C, respectively.

Table 1 List of hydraulic fluid models

	ρ kg/m^3	ν m^2/s (40°C)	ν m^2/s (100°C)
VG 22	866	23.0 ×10^{-6}	4.44 ×10^{-6}
VG 32	869	32.6	5.49
VG 46	872	45.8	6.86
VG 68	875	68.0	8.73
VG 100	882	105.5	11.92

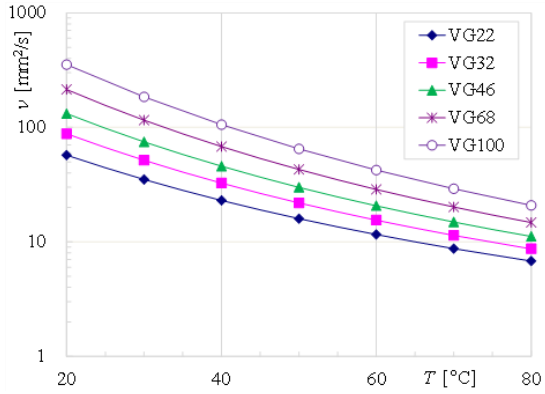

Fig. 2 Kinematic viscosity (ν) vs temperature (T) for oils with VG 22 – 100

3.2 Comparison between ISO and THL solutions

Figures 3–6 present the VG effects on the leakage flow rate (Q_{out}), friction torque (T_f), power loss (L) and maximum temperature (T_{max}) in the film. These figures also include the differences between the ISO and THL solutions under a supply pressure of 21 MPa and a rotational speed of 1500 rpm (25 rps).

As VG decreases, Q_{out} increases and T_f decreases monotonously, mainly because of flow resistance and viscous friction, respectively (Figs. 3 and 4). In Figs. 5 and 6, L and T_{max} were minimised at the mid-VG because L in low and high VGs increased owing to the Q_{out}- and T_f-based losses, respectively.

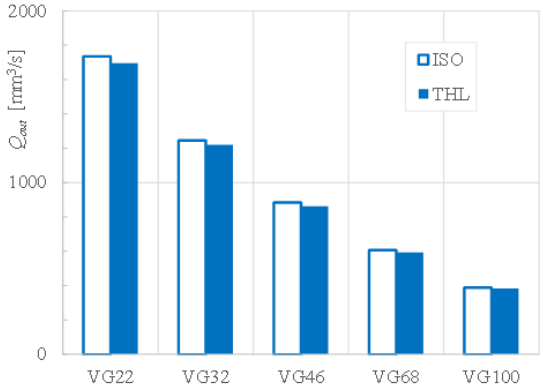

Fig. 3 VG effects on the leakage flow rate (Q_{out}) for VG 22 – 100 (1500 rpm and 21 MPa)

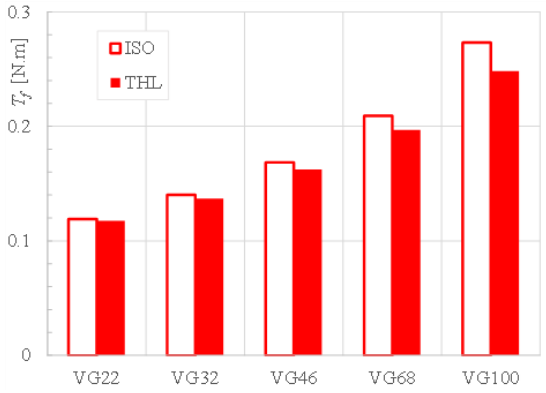

Fig. 4 VG effects on the friction torque (T_f) for VG 22–100 (1500 rpm and 21 MPa)

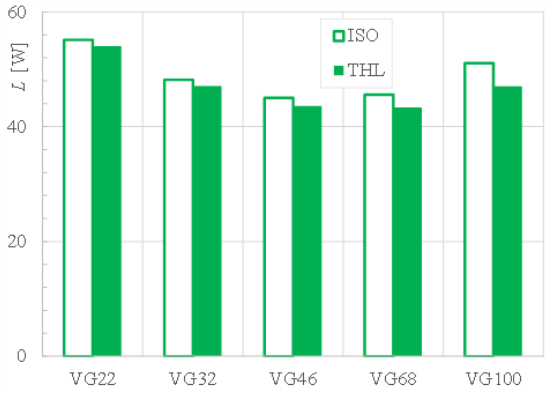

Fig. 5 VG effects on the power loss (L) for VG22 – VG100 (1500 rpm and 21 MPa)

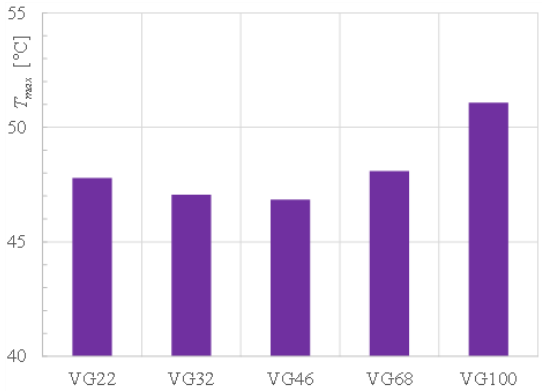

Fig. 6 VG effects on the maximum temperature (T_{max}) for VG 22 – 100 (1500 rpm and 21 MPa)

On comparing the ISO and THL solutions, Q, T_f and L of the ISO were larger than those of the THL. The minimum conditions for T_{max} and L were given at a mid-VG and the conditions were close; however, they were slightly different; T_{max} was minimised with VG 46, whereas, L of THL and ISO were minimised with VG 68 and VG 46, respectively. In any case, L was minimised at a specific VG oil because of the opposite tendency between leakage loss and friction loss against VG.

Figure 7 depicts L in terms of rotational speeds of 900, 1500 and 2100 rpm (15, 25 and 35 rps). The pressure was constant at 21 MPa. VG is represented as ν_0 that is the kinematic viscosity at 40°C for each oil. Under these conditions, L was minimised at a specific ν_0. As the speed increased, L increased and its minimum value shifted to a lower value of ν_0 because of the influence of viscous dissipation in the oil film.

3.3 Relationship with the operating parameter

Figures 8–10 respectively display L, T_{max} and the power loss ratio (L_Q/L) against the normalised operating parameter ($\mu N/p_s$, μ: viscosity $= \rho\nu_0$), corresponding to the operating conditions of p_s = 7–35 MPa and N = 300–1500 rpm (5–25 rps).

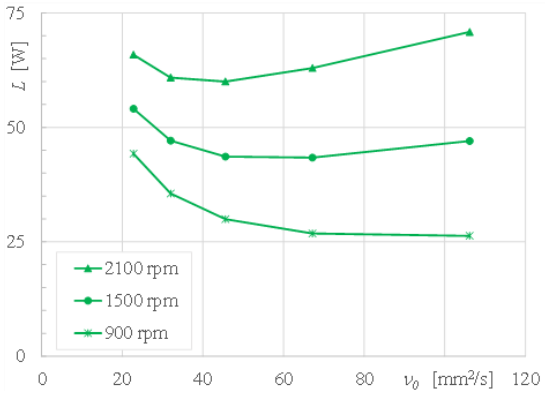

Fig. 7 VG effects on power loss (L) in terms of kinematic viscosity (ν_0) at 40°C (21 MPa)

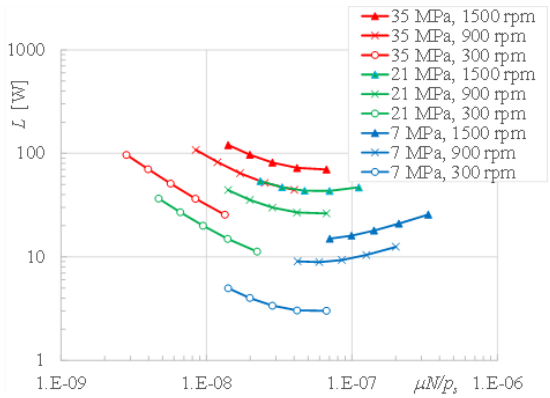

Fig. 8 Relationship between power loss (L) and operating parameter ($\mu N/p_s$)

Under the same μ, $\mu N/p_s$ would have the same value for the combination of (p_s, N) = (7 MPa, 300 rpm), (14 MPa, 600 rpm), (21 MPa, 900 rpm), (28 MPa, 1200 rpm) and (35 MPa, 1500 rpm). In Fig. 8, L is minimised at (21 MPa, 900 rpm) (additionally, (35 MPa, 1500 rpm), (21 MPa, 1500 rpm), (7 MPa, 900 rpm) and (7 MPa, 300 rpm). Hence, L is minimised at $\mu N/p_s \approx (4–7)\times10^{-8}$ over the various operating conditions, corresponding to VG 68–100.

Moreover, in Fig. 9, T_{max} is minimised at the specific conditions: (35 MPa, 1500 rpm) and (21 MPa, 1500 rpm); additionally, (7 MPa, 900 rpm). T_{max} was minimised at $\mu N/p_s \approx 5\times10^{-8}$, corresponding to VG 68. Further, in Fig. 10, all L_Q/L values are located on one curve against $\mu N/p_s$ under these numerical conditions. $\mu N/p_s \approx (4–7)\times10^{-8}$ coincided with $L_Q/L \approx$ 0.4–0.3. These results indicate that an optimum hydraulic oil with a specific VG can be selected for given operating conditions of p_s and N. Otherwise, a preferable operating condition is established to determine a specific VG oil.

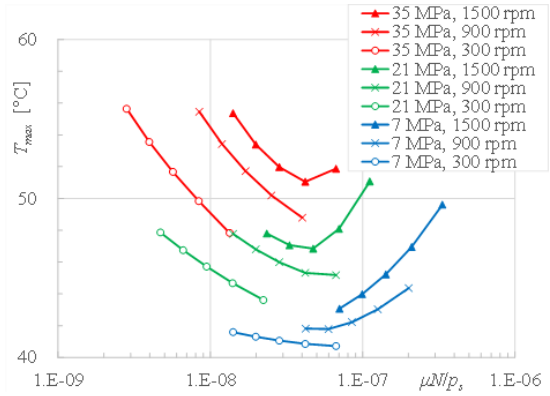

Fig. 9 Relationship between maximum temperature (T_{max}) and operating parameter ($\mu N/p_s$)

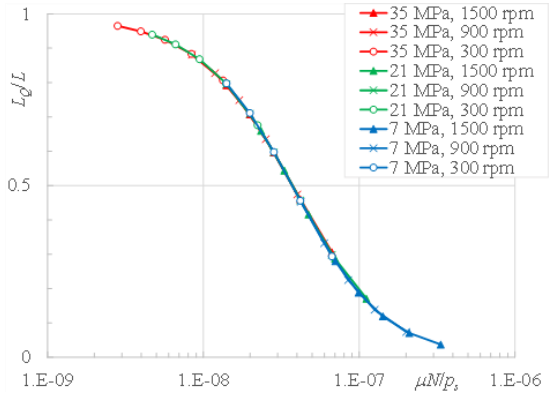

Fig. 10 Relationship between power loss ratio (L_Q/L) and operating parameter ($\mu N/p_s$)

4. Conclusion

Using a THL theory-based slipper model and considering the oil viscosity changes against the temperature distribution in the film, an optimum viscosity of five hydraulic oils with ISO VG 22–100 was explored. Under the operating conditions of a supply pressure of 7–35 MPa and rotational speed of 300–1500 rpm (5–25 rps), an optimum kinematic viscosity was numerically determined in terms of minimised power losses and temperature increment.

Conflicts of Interest

The author declares that there is no conflict of interest.

References

1) H. E. Merritt, Hydraulic Control Systems, Wiley, 1967.
2) T. Kazama, "Transmitted Power of Piping and Wiring in Hydraulic, Pneumatic, and Electric Drive Systems (Considerations for Loss in Pipes and Wires)," JFPS International Journal of Fluid Power System, Vol.13, No.2, pp.9–16, 2020.
3) T. Kazama, "A Comparative Newtonian and Thermal EHL Analysis Using Physical Lubricant Properties," Proc. of 28th Leeds-Lyon Symposium on Tribology, Wien, Austria, pp.435–446, 2002.
4) T. Kazama, "Comparison of Power Density of Transmission Elements in Hydraulic, Pneumatic, and Electric Drive Systems," Mechanical Engineering Letters, Vol.5, pp.19-00139, 2019.
5) Japan Hydraulics and Pneumatics Society, Handbook of Hydraulics and Pneumatics (in Japanese), Ohm-sha, 1989.
6) J. Koralewski, "Influence of Hydraulic Oil Viscosity on the Volumetric Losses in a Variable Capacity Piston Pump," Polish Maritime Research, Vol.18, No.3, pp. 55–65, 2011.
7) A. Yamaguchi, "Motion of the Piston in Piston Pumps and Motors (Experiments and Theoretical Discussion)," JSME International Journal, Ser.B, Vol.37, No.1, pp.83–88, 1994.
8) K. Tanaka, S. Momozono, K. Kyogoku and Y. Fujita, "Effect of Geometric Shape of Piston on Power Loss of Sliding Part Between Piston and Cylinder in Swash Plate Type Piston Pump and Motor," Trans. of JSME (in Japanese), Vol.84, No.868, pp.18–00359, 2018.
9) A. Yamaguchi and M. Tsuchimoto, "Bearing Seal Characteristics of the Oil Film Between a Valve Plate and a Cylinderblock of Axial Piston Pumps," Hydraulics and Pneumatics (in Japanese), Vol.13, No.1, pp.55–60, 1982.
10) M. Ivantysynova and J. Baker, "Power Loss in the Lubricating Gap Between Cylinder Block and Valve Plate of Swash Plate Type Axial Piston Machines," International Journal of Fluid Power, Vol.10, No.2, pp.29–43, 2009.
11) N. Iboshi and A. Yamaguchi, "Characteristics of a Slipper Bearing for Swash Plate Type Axial Piston Pumps and Motors: 1st Report, Theoretical Analysis," Bulletin of JSME, Vol.25, No.210, pp.1921–1930, 1982.
12) J. Chen, J. Ma, J. Li and Y. Fu, "Performance Optimization of Grooved Slippers for Aero Hydraulic Pumps," Chinese Journal of Aeronautics, Vol.29, No.3, pp.814–823, 2016.
13) M. M. Khonsari, "A Review of Thermal Effects in Hydrodynamic Bearings, Part I: Slider and Thrust Bearings," ASLE Transactions, Vol.30, No.1, pp.19–25, 1986.
14) T. Kazama, "Thermohydrodynamic Lubrication Model Applicable to a Slipper of Swashplate Type Axial Piston Pumps and Motors (Effects of Operating Conditions)," Tribology Online, Vol.5, No.5, pp.250–254, 2010.
15) T. Kazama, "Thermohydrodynamic Lubrication Model of a Slipper in Swashplate Type Axial Piston Machines–Validation Through Experimental Data," International Journal of Hydromechatronics, Vol.1, No.3, pp.259–271, 2018.
16) T. Kazama, "Numerical Simulation of a Slipper Model with Multi-Lands and Grooves for Hydraulic Piston Pumps and Motors in Mixed Lubrication," Lubricants, Vol.7, No.7, pp.55, 2019.
17) T. Kazama, T. and A. Yamaguchi, "Optimum Design of Bearing and Seal Parts for Hydraulic Equipment," Wear, Vol.161, No.1/2, pp.161–171, 1993.
18) T. Kazama, T. and A. Yamaguchi, "Application of a Mixed Lubrication Model for Hydrostatic Thrust Bearings of Hydraulic Equipment," J. of Tribology, Trans. of ASME, Vol.115, No.4, pp.686–691, 1993.